Journal of Materials Chemistry A

ROYAL SOCIETY OF CHEMISTRY

PAPER

View Article Online
View Journal | View Issue

Check for updates

Cite this: *J. Mater. Chem. A*, 2022, **10**, 18822

Highly stable Pebax® Renew® thin-film nanocomposite membranes with metal organic framework ZIF-94 and ionic liquid [Bmim][BF_4] for CO_2 capture†

Lidia Martínez-Izquierdo, [ab] Carlos Téllez [ab] and Joaquín Coronas *[ab]

Received 17th May 2022
Accepted 7th August 2022

DOI: 10.1039/d2ta03958c

rsc.li/materials-a

Ionic liquid (IL) [Bmim][BF_4] and metal organic framework (MOF) ZIF-8 and ZIF-94 nanoparticles were incorporated into polymer Pebax® Renew® 30R51 to obtain highly efficient thin-film nanocomposite (TFN) membranes, *ca.* 300 nm thick. ZIF-94 particles were synthesized *via* a solvent assisted ligand exchange (SALE) from nano ZIF-8. To fabricate the membranes, the weight percentage of [Bmim][BF_4] was firstly varied from 5 to 20 wt% to find the optimal IL content (10 wt%). Besides, ZIF-8 and ZIF-94 nanoparticles were separately incorporated (from 10 to 20 wt%) into the Pebax®/IL matrix to enhance the CO_2 separation performance. Compared with the pristine Pebax® thin film composite (TFC) membrane, the IL (10 wt%) increased the CO_2 permeance by 27% to 629 GPU and the CO_2/N_2 separation selectivity by 7% to 29 due to the enhancement in CO_2 mass transport. After the incorporation of ZIFs, the CO_2 permeance increased by 51% to 751 GPU and by 65% to 819 GPU, with 15 wt% loadings of ZIF-8 and ZIF-94, respectively, although the CO_2/N_2 separation selectivity decreased by 7% to 25 in both cases. Additional characterization was also carried out by the calculation of the permeation apparent activation energies for CO_2 and N_2 as well as the study of the long-term stability for up to 18 days. This demonstrated that the incorporation of the MOF enhanced the stability of the IL in the membrane, rendering it 55% and 35% more permeable (611 GPU) than the bare polymer and the membrane with only IL, respectively, while maintaining a CO_2/N_2 separation selectivity of 25.

1. Introduction

To reach the international target of net-zero CO_2 emissions by 2050, the use of green and renewable energy has drawn remarkable attention. Moreover, the development of technologies capable of separating and capturing CO_2 is also the scope of many studies.[1–3] Among the existing methods of CO_2 separation (*e.g.* amine absorption, cryogenic distillation and adsorption), membrane technology has many advantages such as simple processing equipment, operating flexibility, high reliability, small footprint, low energy requirement and environment friendliness.[4–7] However, current dense membranes suffer from very low CO_2 permeance, which makes them noncompetitive for industrial applications.[8] To achieve efficient separations, exceeding the Robeson trade-off relationship between permeability and selectivity,[9] thin film composite membranes (TFC) must be prepared with a very thin selective layer (with a thickness lower than 1 μm).

In addition, the introduction of nanoparticles with molecular sieving properties within the polymer matrix is also regarded to improve the gas separation performance.[10,11] A variety of nano-fillers have been proved to enhance the separation performance of membranes, *e.g.* carbon derivatives,[12–14] zeolites[15,16] and metal–organic frameworks (MOFs).[17–20] Among them, MOFs and in particular zeolitic imidazolate frameworks (ZIFs), a sub-class of MOF, are being widely studied due to their improved affinity to the polymer matrix.[21] Such increased compatibility in MOF-type fillers is possible due to the presence of organic linkers within their structure.[22] Besides solid nano-fillers, the incorporation of liquids (*e.g.* ionic liquids, ILs) with increased mass transport in comparison to the polymer matrix is also the subject of many studies.[23,24] Such increment in the mass transport velocity allows higher permeances of CO_2 through the membrane and more efficient separations.[25] Interestingly, this approach has been followed to prepare a mix of both solid particles and ILs, which is now gaining special attention due to the possibility of boosting the gas separation performance of membranes by combining their properties. Lu *et al.*[26] prepared PIM-1 mixed matrix membranes (MMMs) with

[a]*Instituto de Nanociencia y Materiales de Aragón (INMA), CSIC-Universidad de Zaragoza, Zaragoza 50018, Spain. E-mail: coronas@unizar.es*

[b]*Chemical and Environmental Engineering Department, Universidad de Zaragoza, Zaragoza 50018, Spain*

† Electronic supplementary information (ESI) available. See https://doi.org/10.1039/d2ta03958c

an IL-modified UiO-66-NH_2 filler. They found that the IL improved not only the hydrophobicity of UiO-66-NH_2, thus facilitating the dispersion of the particles into the polymer, but also the affinity between the MOF and polymer. By using this strategy, they were able to reduce the non-selective interfacial defects with the corresponding enhancement of the gas separation behavior. Attempts to combine the advantages of solid and liquid additives have also been made with carbonaceous based particles. Huang *et al.*[27] prepared a Pebax®/ionic liquid modified graphene oxide (GO-IL) MMM with enhanced CO_2 separation performance. They found that the IL improved both the CO_2 solubility and the CO_2/gas selectivity of the MMMs. This allowed them to increase the CO_2/N_2 selectivity and the CO_2 permeability over 90% and 50%, respectively, compared to the pristine membrane. Jomekian *et al.*[28] prepared surface IL-modified Pebax® 1657 membranes filled with ZIF-8 particles. These MMMs with a 13 μm thick Pebax® layer on a PES support had an insignificant content of IL, whose mission was to functionalize the Pebax® surface. This caused an increase in the CO_2 selectivity in the membranes with ZIF-8 due to the better interaction between the components of the MMM. Such improvement in the interaction of the filler with the polymer due to the presence of an ionic liquid has also been reported in other works.[29,30]

ZIF-94, also named as SIM-1, is a zeolitic imidazolate framework synthesized from Zn atoms and 4-methyl-5-imidazolate-carboxaldehyde linkers sharing the same SOD type topology as ZIF-8.[31,32] In the present work, ZIF-94 nanoparticles were combined with the anionic liquid 1-butyl-3-methylimidazolium tetrafluoroborate [Bmim][BF_4] and incorporated into a Pebax® Renew® polymer to prepare thin film nanocomposite (TFN) membranes. These, unlike a typical dense MMM, are supported MMMs whose thin selective layer incorporates nanoparticles. Pebax® is a commercial brand of block copolymer elastomers built up of rigid polyamide blocks and soft polyether blocks (PEBA). Pebax® Renew® code was chosen for this project due to its renewable nature (it contains 41% of renewable carbon, measured by ASTM D6866 as reported by Arkema in the corresponding data sheet), and similar composition to highly studied Pebax® 1657, thus anticipating similar separation properties. As previously noted by Neves *et al.*[33] and Jiang *et al.*,[34] the IL [Bmim][BF4] was selected over other imidazolium-based ionic liquids due to its improved performance in gas separation, ideal to demonstrate the membrane concept developed in this work. To the best of our knowledge this is a non-studied system;[35,36] the closest situation includes Pebax® 1657/graphene oxide-IL TFN membranes, whose operation stability was studied for only up to 28 h.[27,37] Besides, it is worth mentioning that the ZIF-94 crystals used for this research were prepared *via* a solvent assisted ligand exchange (SALE) reaction using 1-butanol as reaction medium and nano-ZIF-8 as precursor material. With this strategy, the obtained ZIF has the controlled particle size of ZIF-8 and the high CO_2-philicity of ZIF-94 due to the aldehyde group in its ligand. This SALE method avoids the use of other toxic solvents such as tetrahydrofuran (THF) or dimethylformamide (DMF),[38] while taking advantage of the easy control of ZIF-8 synthesis in terms of particle size and geometry. ILs and MOFs have been previously incorporated together into PEBA membranes for gas separation.[23,39,40] However, the vast majority of reports available concerning this topic are related to self-supported MMMs. The intent of this research is to prepare a new generation of TFN membranes for CO_2/N_2 and CO_2/CH_4 separation with improved gas separation performance over time.

2. Experimental

2.1. Materials

Zinc nitrate hexahydrate ($Zn(NO_3)_2 \cdot 6H_2O$) and 2-methylimidazole (2-mIm) were purchased from sigma Aldrich. 4-Methyl-5-imidazole-carboxyaldehyde was purchased from Acros Chemicals. The ionic liquid, 1-butyl-3-methylimidazolium tetrafluoroborate [Bmim][BF_4] (Scheme 1), was purchased from Fisher Scientific, Spain. Polysulfone (Udel® P-3500 LCD) was purchased from Solvay Advanced Polymers. Poly[1-(trimethylsilyl)prop-1-yne] (PTMSP) was purchased from Fluorochem, United Kingdom. Polyether-*block*-amide, Pebax® Renew® 30R51 (with a percentage of renewable carbon of 41%) in the form of pellets was kindly provided by Arkema, France. This is a thermoplastic elastomer

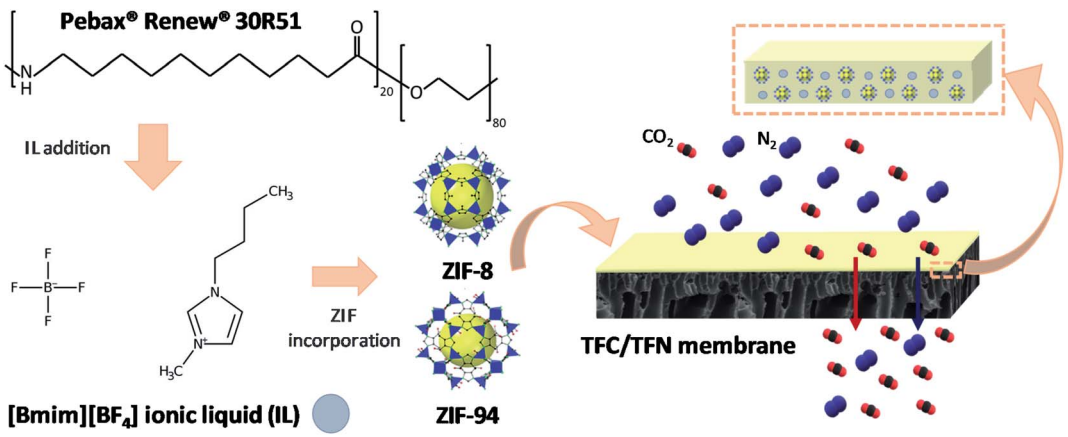

Scheme 1 Schematic diagram of Pebax 30R51, [Bmim][BF4] IL and ZIF-8 and ZIF-94 structures (corresponding to hybrid ZIF ZIF-94/ZIF-8) and the gas separation mechanism through a TFC/TFN membrane.

made from flexible polyether and rigid polyamide based on renewable resources. The solvents, methanol (MeOH), *N*-methyl-2-pyrrolidone (NMP), 1-propanol (1-PrOH) and 1-butanol (1-ButOH) were purchased from Análisis Vínicos, Panreac, Labbox and Scharlab, Spain, respectively. All gases used for the separation tests were of research grade (greater than 99.995% of purity) and supplied by Abelló Linde S. A., Spain. All gases, polymers and solvents were used as received.

2.2. Methods

2.2.1. Synthesis of ZIF-8 (20 nm). ZIF-8 nano-particles were synthesized according to a previously reported method[41] with some deviations. Typically, 1.467 g of $Zn(NO_3)_2 \cdot 6H_2O$ (4.93 mmol) and 3.245 g of 2-mIm (39.52 mmol) were first dissolved in 150 mL of MeOH, respectively. Once dissolved, the ligand solution (2-mIm) was poured into the metal solution under stirring. The resulting solution was further stirred for 30 min at room temperature (RT), followed by centrifugation at 9000 rpm for 10 min and several washing steps with MeOH. The final product was then dried and activated at 40 °C overnight.

2.2.2. Synthesis of ZIF-94: original route (OR) and solvent assisted ligand exchange (SALE). In order to compare and confirm the successful ligand exchange in the synthesis of ZIF-94 from ZIF-8 nanoparticles, ZIF-94 powder was firstly synthesized according to a previous two-step procedure.[42] Initially, the metal solution was prepared by dissolving zinc acetate dihydrate (7.2 mmol) and NaOH (14.4 mmol) in 6 mL of MeOH. The ligand solution was prepared by dissolving the stoichiometric amount of 4-methyl-5-imidazole-carboxyaldehyde (14.4 mmol) in 15 mL of THF. Once the metal and ligand solutions were prepared, the MeOH solution was poured into the THF solution under vigorous stirring. Reaction was carried out at RT for 16 h. Afterwards, ZIF-94 powder was collected by centrifugation at 9000 rpm for 10 min and washed several times with fresh MeOH under the same conditions. Finally, ZIF-94 crystals were activated by refluxing with 50 mL MeOH per g ZIF-94 for 1.5 h and collected by centrifugation. The resulting product was dried overnight at RT and named ZIF-94 (OR).

The solvent assisted ligand exchange (SALE) reaction was carried out according to a previously reported method by Marti *et al.*[43] Briefly, 0.323 g of 4-methyl-5-carboxyaldehyde (2.94 mmol) were first dissolved in 20 mL of 1-ButOH. Then, 100 mg of nano ZIF-8 were suspended in the precursor solution and stirred at RT for 24 h. The resulting product was collected by centrifugation at 9000 rpm for 10 min and washed several times with fresh 1-ButOH under the same conditions. The final crystals were dried and activated at 40 °C overnight. The ZIF-94 particles obtained this way were named ZIF-94 (SALE).

2.2.3. Membrane preparation. PSF supports were prepared by casting followed by phase inversion.[44] First, PSF pellets (15 wt%) were dissolved in NMP at room temperature under stirring overnight. After complete degasification, the PSF solution was cast onto a Teflon plate using an Elcometer 4340 Automatic Film Applicator at a thickness of 250 μm and with a casting speed of 0.05 m s^{-1}. After casting, the supports were immersed in a water bath at room temperature for 1 h, transferred to a deionized water bath overnight, rinsed with isopropanol and dried at 40 °C overnight.

A PTMSP gutter layer was spin-coated (Fig. 1) onto the PSF supports to avoid the penetration of the selective layer. Firstly, a PTMSP solution was prepared dissolving at room temperature the polymer in *n*-hexane in a concentration of 2 wt%. Once dissolved, 0.6 mL of this solution was poured onto the support, previously attached to the spinner by vacuum, and spun at 2500 rpm for 20 s. The supports with the gutter layer were placed in an oven at 40 °C for 1 h to evaporate the residual solvent.

The final selective layer was also spin-coated onto the PTMSP/PSF supports at 2500 rpm for 20 s. For this purpose, a Pebax® Renew® solution was prepared dissolving under reflux 0.2 g of the polymer in 9.8 g of a 1-PrOH/1-ButOH (3/1 v/v) mixture at 80 °C for 2 h. To avoid gelation, the polymer solution was immersed in a water bath at 45 °C. Finally, 0.6 mL of this solution was poured onto the PTMSP/PSF support and spun to obtain the Pebax®Renew®/PTMSP/PSF TFC membrane. Similarly, Pebax®Renew® (IL)/PTMSP/PSF membranes were prepared by adding the IL (from 5 to 20 wt%, respect to the

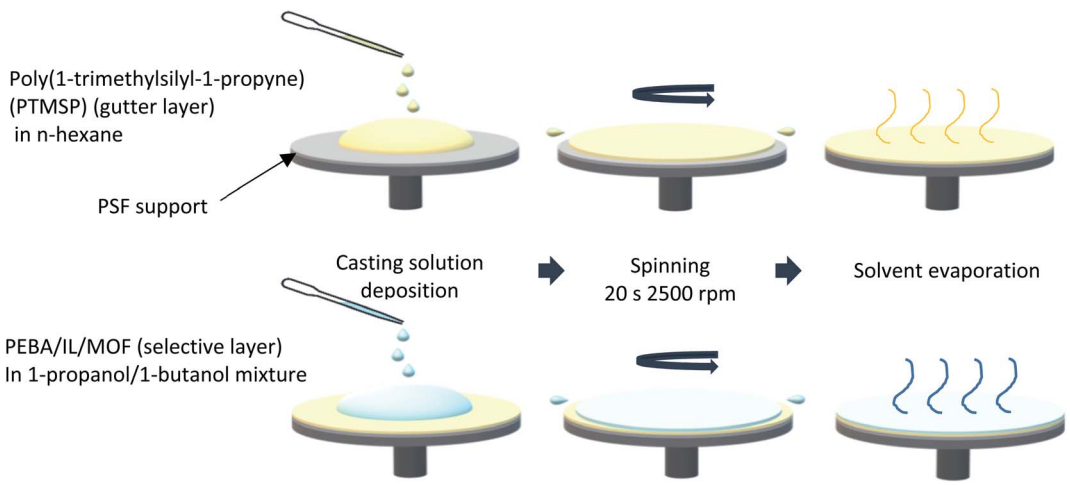

Fig. 1 Spin-coating method: from the coating of the PTMSP gutter layer to that of the PEBA/IL/ZIF in one step.

polymer) to the Pebax® solution once cooled down. Solutions of Pebax® with the IL were stirred at 45 °C for 1 h before spinning. The TFC membranes prepared this way were abbreviated as TFC_PEBA(*X*IL), where *X* is the IL concentration. After testing the TFC_PEBA(*X*IL) membranes in the gas separation set up, the optimal condition (10 wt% of IL, see section 3.3.1.) was selected to prepare the TFN membranes with the nanocrystals of ZIF-8 and ZIF-94 prepared by the SALE reaction. In this case, the polymer was dissolved in 2/3 of the total solvent under the same conditions while different amounts of ZIF-8 and ZIF-94 particles (from 10 to 20 wt%, respect to the polymer) were suspended in the remaining solvent (1/3 of the total) using an ultrasonic bath. Once the polymer was dissolved and cooled down to 40–45 °C, the IL was added to the solution and stirred for 5 min before incorporating the ZIF suspension. Casting suspensions with the IL and ZIFs were stirred for 1 h at 45 °C before spinning. The membranes prepared this way were named as TFN_PEBA(10IL)_ZIF8(*Y*) and TFN_PEBA(10IL)_ZIF94(*Y*), where *Y* is the wt% concentration of ZIF-8 and ZIF-94. All the membranes were placed in an oven at 40 °C for 18 h after spinning to remove any residual solvent.

2.2.4. ZIFs and membranes characterization. Scanning electron microscopy (SEM) images of ZIF powders and membranes were obtained using an Inspect F50 model scanning electron microscope (FEI), operated at 10 kV. This instrument was also used for measuring (at 5–6 different positions along the membrane) the thickness of the selective skin layer. Cross-sections of membranes were prepared by freeze-fracturing after immersion in liquid N_2 and subsequently coating with Pd. Thermogravimetric analyses (TGA) and differential thermogravimetry (DTG) were carried out using a Mettler Toledo TGA/STDA 851e. Small amounts of ZIF powder (~3 mg) placed in 70 μL alumina pans were heated under an airflow (40 cm^3 (STP) min^{-1}) from 35 to 700 °C at a heating rate of 10 °C min^{-1}. ZIFs were also characterized by Fourier transform infrared spectroscopy (FTIR-ATR), which was performed with a Bruker Vertex 70 FTIR spectrometer equipped with a DTGS detector and a Golden Gate diamond ATR accessory. The spectra were recorded by averaging 40 scans in the wavenumber range of 4000–600 cm^{-1} at a resolution of 4 cm^{-1}. ZIF crystallinity was analyzed by X-ray diffraction (XRD) using a Panalytical Empyrean equipment with CuKα radiation ($\lambda = 0.154$ nm), over the range of 5° to 40° at a scan rate of 0.03° s^{-1}. The N_2 adsorption isotherms of the ZIFs prepared were measured using a Micromeritics Tristar 3000 at 77 K. Prior to the isotherm measurement, the samples were degassed for 8 h under vacuum at 200 °C, using a heating rate of 10 °C min^{-1}. The specific surface area (SSA) of the porous materials was calculated by the Brunauer–Emmett–Teller (BET) method.

2.2.5. Gas separation tests. Membranes were cut and placed in a module consisting of two stainless steel pieces and a 316LSS macro-porous disk support (Mott Co.) with a 20 μm nominal pore size. Membranes, 2.12 cm^2 in area, were gripped inside with Viton O-rings. To control the temperature of the experiment (in the 25–50 °C range), which has an effect on gas separation, the permeation module was placed in a UNE 200 Memmert oven. In this work, the gas separation measurements were carried out by feeding the post-combustion gaseous mixture CO_2/N_2 (15/85 cm^3 (STP) min^{-1}) and the mixture CO_2/CH_4 (50/50 cm^3 (STP) min^{-1}) to the feed side at an operating pressure of 3 bar to favor CO_2 permeation. Gas flows of the mixtures were controlled by mass-flow controllers (Alicat Scientific, MC-100CCM-D). The permeate side of the membrane was swept with a 4.5 cm^3 (STP) min^{-1} of He, at atmospheric pressure (~1 bar) (Alicat Scientific, MC-5CCM-D). The stage cut (θ), defined as the ratio of permeate to feed flow rate is *ca.* 2%. Concentrations of CO_2, N_2 and CH_4 in the outgoing streams (permeate side) were analyzed online by an Agilent 3000A micro-gas chromatograph. Permeances of CO_2, N_2 and CH_4 were calculated in GPU (gas permeance unit, 10^{-6} cm^3 (STP) cm^{-2} s^{-1} $cmHg^{-1}$), once the steady state of the exit stream was reached. The CO_2/N_2 and CO_2/CH_4 separation selectivities were calculated as the ratios of the corresponding permeances.

3. Results

3.1. Characterization of ZIF-8 and ZIF-94

ZIF-8 and ZIF-94 were synthesized in order to be used as loadings for Pebax® Renew® thin film nanocomposite (TFN) membranes. As seen in Fig. 2a and b, the average particle sizes of synthesized ZIF-8 and ZIF-94 (SALE) were 30 ± 5 nm and 48 ± 6 nm, respectively. Furthermore, the ZIF-94 particles have a less round shape and a larger particle size which may be related to an Ostwald ripening effect during the SALE.[45] To confirm the ligand exchange, TGA analyses were carried out from 35 to 700 °C under air atmosphere. Results (Fig. 2c) revealed that the particles synthesized from ZIF-8 (ZIF-94 (SALE)) had the same degradation behavior that the ones synthesized by the original route (ZIF-94 (OR)), which besides differs from the degradation behavior of ZIF-8. While the maximum degradation of ZIF-94 nanoparticles takes place between 375 °C and 400 °C, the one of ZIF-8 happens at a higher temperature, *ca.* 450 °C. It is also worth mentioning that the ZIF-8 weight loss is more abrupt than those of ZIF-94 OR and SALE. Furthermore, the weight loss between 100–200 °C in the ZIF-94 (OR) thermogram suggests that there is still some remaining solvent from the ZIF synthesis. Conversely, the ZIF-94 (SALE) particles do not present such weight loss, indicating that the powder was successfully activated, probably due to the washing produced during the SALE process. The crystallinity and purity of the ZIF particles were confirmed by XRD. The patterns of the simulated ZIFs and the synthesized ones are plotted together for comparison in Fig. 2d. As seen in this figure, the peak positions match well with those of the simulated ZIF-8. In fact, as both ZIFs share the same SOD type structure, the simulated patterns of ZIF-8 and ZIF-94 can be considered the same.[32,46] The FTIR-ATR spectra of ZIFs are depicted in Fig. 2e, revealing a similar spectrum for ZIF-94 (SALE) than for ZIF-94 (OR), with the main bands of ZIF-94 at 1660 cm^{-1}, which corresponds to the aldehyde group (–CHO),[47] and 1496 cm^{-1}, related to the C=C bond. Besides the similar FTIR spectra of ZIF-94 (SALE) and (OR), the absence of the main bands of ZIF-8 at 1147 cm^{-1} and 993 cm^{-1} (both corresponding to the C–N bond)[48] agree with the successful ligand exchange. The N_2 adsorption isotherms and BET SSA values also confirm

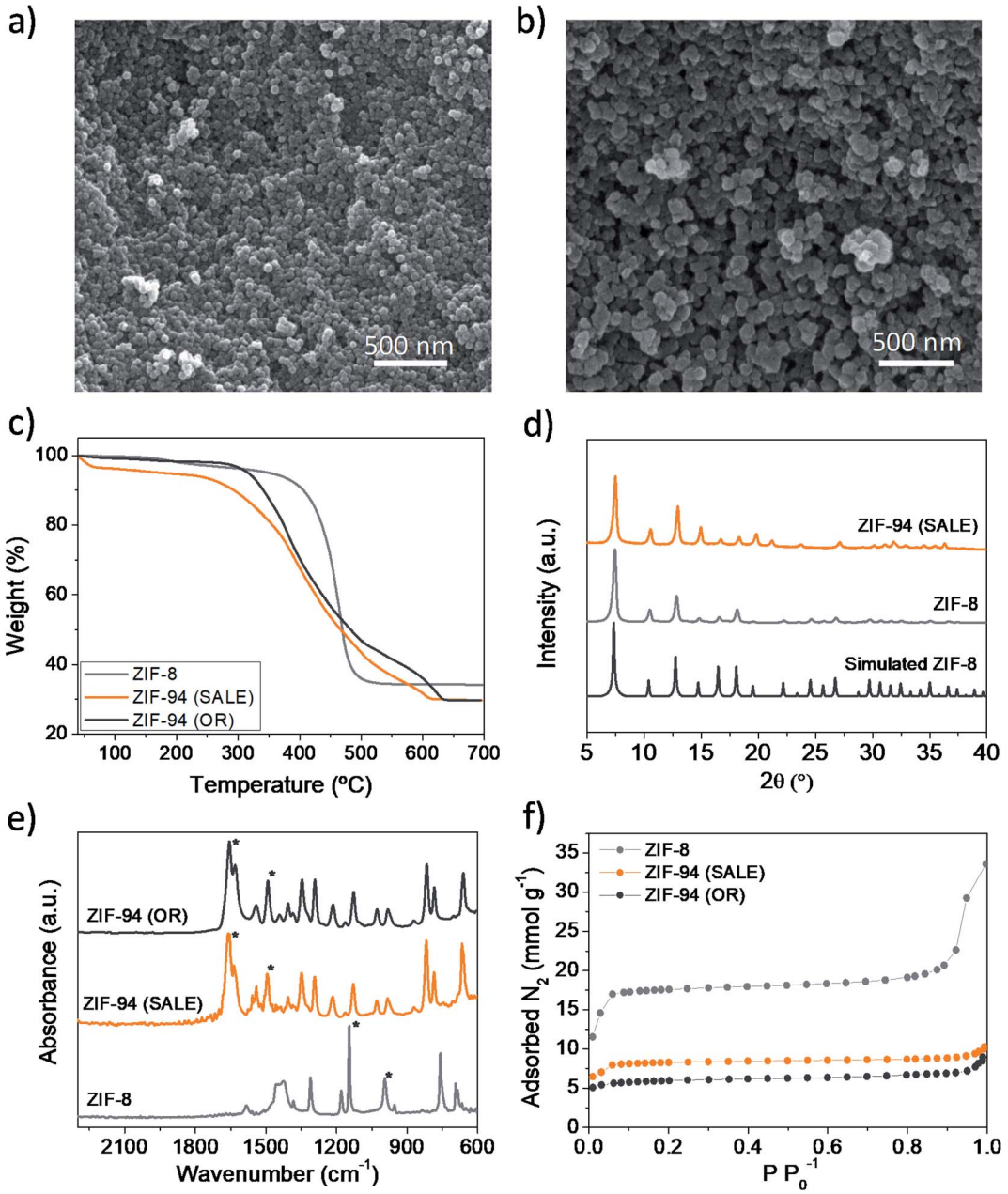

Fig. 2 Characterization of ZIF particles. SEM images of ZIF-8 (a) and ZIF-94 (SALE) (b), thermal properties of ZIF-8, ZIF-94 (OR) and ZIF-94 (SALE) powders (c), XRD patterns of ZIF-94 (SALE), ZIF-8 and the simulated ZIF-8 (d), ATR-FTIR spectra of ZIFs (e) and N_2 adsorption isotherms at −196 °C of ZIF-8, ZIF-94 (OR) and ZIF-94 (SALE) particles (f).

the ligand exchange (Fig. 2f). In this case, the BET SSA decreases from 1350 $cm^2\ g^{-1}$ for the ZIF-8 to 464 $cm^2\ g^{-1}$ for the ZIF-94 (OR) and to 645 $cm^2\ g^{-1}$ for the ZIF-94 (SALE), which is in accordance with the literature for synthesized ZIF-94 particles.[47,49] However, these values suggest that the conversion of ZIF-8 into ZIF-94 was high but not complete with a remain of the ZIF-8 composition responsible for the larger value of BET SSA for ZIF-94 (SALE) as compared to that of the as-made ZIF-94. Furthermore, Fig. 2f reveals the type I IUPAC classification of adsorption isotherms for both products, thus indicating dominant microporosity of these materials.[50]

3.2. Characterization of membranes

The thicknesses of the PTMSP and Pebax® layers were measured by SEM. Cross-sections of the membranes are depicted in Fig. 3a–d. As observed in all images, a very thin layer of Pebax® Renew® (300 nm) was coated on top of a 1 μm thick PTMSP gutter layer. The PTMSP gutter layer is placed between the support and the selective layer to avoid the polymer penetration of the latest into the support,[51] which would be detrimental for the final gas separation performance unnecessarily increasing the transport resistance. Indeed, PTMSP constitutes a poorly selective and highly permeable glassy polymeric

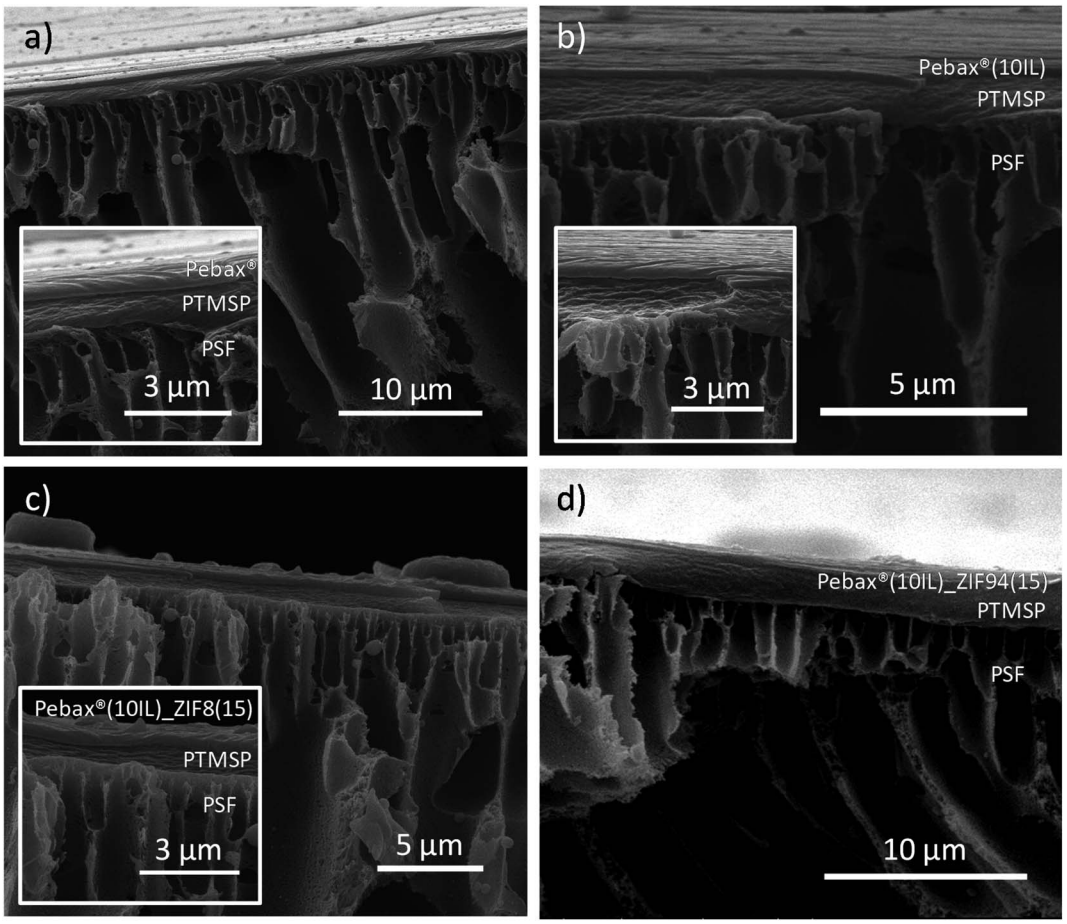

Fig. 3 Cross-section SEM images of some of the Pebax® Renew® TFC membranes prepared in this work. (a) TFC_PEBA, (b) TFC_PEBA(10IL), (c) TFN_PEBA(10IL)_ZIF8(15) and (d) TFN_PEBA(10IL)_ZIF94(15).

material and it is expected that its contribution to the final resistance to the gas permeation is negligible.[52] Further characterization was carried out to study the stability and crystallinity of the membranes by TGA, DTG and XRD analyses. With this purpose, a dense Pebax® Renew® membrane was prepared *via* casting-solution and the results are depicted in Fig. S1a and b,† respectively. As seen in Fig. S1a,† the Pebax® Renew® polymer is stable up to 300 °C and it is degraded completely at 540 °C. In this figure, two degradation steps are appreciable. The first one (from 300 °C to 460 °C) is related to the major thermal degradation of the polymer, whereas the second (from 460 °C to 540 °C) corresponds to the carbonization of the degraded polymer chains.[53] The XRD pattern shown in Fig. S1b† depicts the semicrystalline nature of Pebax® type copolymers.[17,54,55] In the case of this renewable code, three main crystalline peaks are noticeable in the diffractogram at 7.6°, 20.4° and 24.3° 2θ values, the first and second corresponding to the PEO and the third to the PA11 segments.[56]

3.3. Gas separation performance

3.3.1. Incorporation of ionic liquid [Bmim][BF_4]. Before attacking the effect of MOFs, the optimal concentration of ionic liquid [Bmim][BF_4] in the Pebax® Renew® composite membrane was studied by incorporating different weight percentages (from 5 to 20 wt%, respect to the polymer) into the polymer solution. The results in Fig. 4a and Table S1† indicate that the best separation performance was obtained for the membranes with a 10 wt% of IL loading, achieving a CO_2 permeance of 629 ± 74 GPU and a CO_2/N_2 selectivity of 29 ± 1. The increase in CO_2 permeance can be due to the fact that the IL, which is in liquid state, is placed in low quantity between the polymer chains increasing mobility and free volume.[57] Furthermore, the increment of CO_2 permeace can be also attributed to the increase of CO_2 solubility in the membrane, induced by the presence of the IL which has a strong affinity with CO_2. From 10 wt% of IL, the CO_2 permeance decreased progressively to values below that of the bare TFC membrane (438 ± 66 *vs.* 497 ± 71 GPU of CO_2 and a CO_2/N_2 selectivity of 25 ± 1 *vs.* 27 ± 3 for the membranes with a 20 wt% and 0 wt% of IL, respectively). The decrease of CO_2 permeance with the increment of IL up to 20 wt% can be due to the fact that ionic liquids have a relatively high viscosity, which may result in slow mass transfer rates.[58] In addition, as the amount of the liquid phase increases, there may be regions in the membrane in which the transport happens through a liquid medium with worse interfacial contact with the polymer (responsible of the decrease of

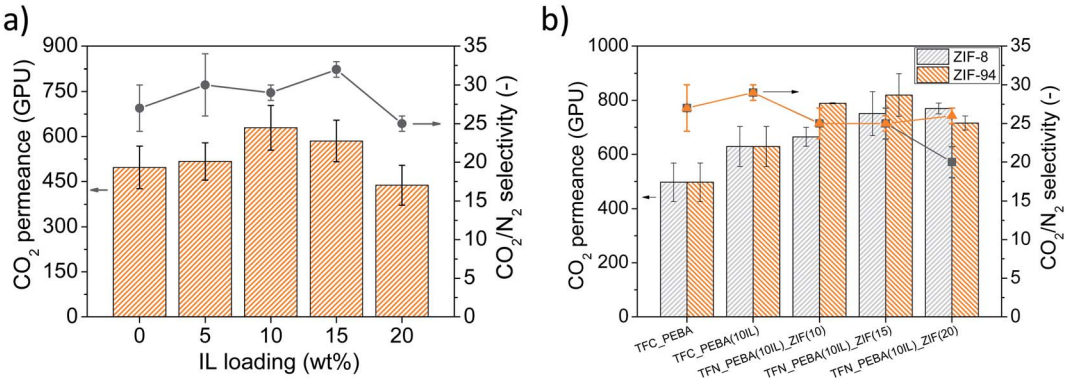

Fig. 4 Gas separation performance of the TFC membranes prepared with different IL content dispersed on Pebax® Renew® (a) and CO_2/N_2 separation performance of the membranes with 10 wt% of IL and ZIFs (ZIF-8 and ZIF-94 (SALE)) (b). Measured at 35 °C and 3 bar. Error bars come from the testing of at least 3 different membranes prepared under the same conditions.

CO_2/N_2 selectivity) and less diffusivity than the bare polymer (responsible of the decrease of CO_2 permeance). Analogous effects have been reported for the CO_2/N_2 mixture at much higher IL concentrations when operating with dense membranes.[59] Therefore, a maximum IL loading of 10 wt% was chosen to prepare the membranes with ZIFs.

3.3.2. Incorporation of ZIF-8 and ZIF-94 (SALE). As explained before in the experimental section, two different ZIF nanoparticles (ZIF-8 and ZIF-94) were incorporated into the Pebax® Renew® nanocomposite membranes. First, ZIF-8 nanocrystals with an average size of *ca.* 30 nm were loaded at different concentrations (10, 15 and 20 wt%, respect to the polymer) into the TFC_PEBA(10IL) membranes with 10 wt% IL. As expected, the CO_2 separation performance of the membranes after the incorporation of ZIF-8 increased synergistically, reaching the highest CO_2 permeance at 20 wt% of ZIF-8 loading (770 ± 20 GPU) together with the lowest CO_2/N_2 selectivity (20 ± 2) (Fig. 4b and Table S2†). The chemical similarity between the ZIFs and the IL, having both imidazole groups, suggests good interaction between them justifying the mentioned synergistic behavior. This will also contribute to the enhance of the IL stability assessed in the long term CO_2/N_2 separation experiments (see below). In addition, the incorporation of the IL into the Pebax®/ZIF-8 matrix also contributes to improve the MOF–polymer interface, thus enhancing the CO_2/N_2 separation performance of the MMM, as expected.[28] The decrease of selectivity at high loadings can be attributed to the aggregation of particles inside the Pebax® matrix, which may create a non-ideal interface between the polymer and the ZIF crystals.[60] It is also worth mentioning that ZIF-8 particles are hydrophobic whereas Pebax® polymer is hydrophilic. This fact can also be detrimental to the gas separation performance of the membranes, since the lack of compatibility between the polymer and the filler may create voids in the polymer matrix which results in the loss of separation efficiency. Therefore, it is expected that the replacement of these hydrophobic particles with hydrophilic ones (*i.e.* ZIF-94) would be beneficial to achieving a significant increase in the gas separation performance. ZIF-94, as ZIF-8, is a Zn^{2+} based MOF but with 4-methyl-5-imidazolate-carboxyaldehyde as organic linker, which makes it hydrophilic as compared to ZIF-8 (ref. 48 and 61) and also more inclined to adsorb CO_2 (the CO_2 uptake of ZIF-8 at 298 K and 1 bar being 0.7 mmol g^{-1} (ref. 62 and 63) and that of ZIF-94, 2.4–2.9 mmol g^{-1} (ref. 47)). The same amounts of ZIF-94 have been tested in membranes with a 10 wt% of IL and the results can be also observed in Fig. 4b and Table S3.† As expected, the membranes prepared with ZIF-94 reached higher permeation values up to 15 wt% of loading, this being the highest CO_2 permeance value obtained in this work (820 ± 79 GPU) and with a CO_2/N_2 selectivity of 25 ± 1. Such CO_2/N_2 selectivity value is only slightly lower than that obtained with the less permeable (497 ± 71 GPU) bare TFC_PEBA membrane (27 ± 3) and with the membrane with a 10 wt% of IL but without ZIF (TFC_PEBA(10IL), 29 ± 1 with 629 ± 74 GPU CO_2 permeance. As for ZIF-8 particles, at high loadings of ZIF-94, the CO_2 permeance decreases due to particle agglomeration reaching a value of 716 $\pm$ 26 GPU at 20 wt% of ZIF-94. Nevertheless, the CO_2/N_2 selectivity is maintained (26 ± 1).

3.3.3. Gas separation as a function of temperature. To study the behavior of the Pebax® Renew® TFC and TFN membranes with temperature, gas separation experiments were carried out at 25, 35 and 50 °C with the membranes chosen as optimal in this work: TFC_PEBA, TFC_PEBA(10IL) and TFN_PEBA(10IL)_ZIF94(15) (Fig. 5). This study is important since the temperature usually improves the membrane permeance with the limitation of the loss of separation selectivity and the membrane stability. Only ZIF-94 was tested for these experiments due to its better performance as compared to ZIF-8. With the obtained data, the apparent activation energies of permeation were calculated using the Arrhenius equation as reported elsewhere (eqn (1)):[44,64]

$$P = P_0 \exp\left(\frac{-E_p}{RT}\right) \quad (1)$$

where P is the CO_2 or N_2 permeance in GPU, P_0 is the pre-exponential factor in GPU, E_p is the apparent activation energy for permeation in J mol^{-1}, R is the ideal gas constant in J mol^{-1} K^{-1} and T the temperature in K. It is expected that the

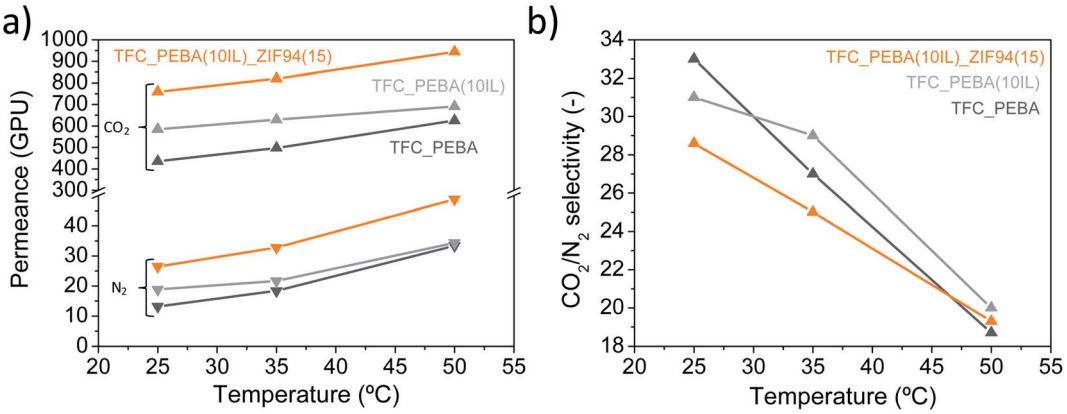

Fig. 5 Gas separation performance as a function of temperature. Measured at 25, 35 and 50 °C and 3 bar. (a) CO_2 and N_2 permeances and (b) CO_2/N_2 selectivity.

sensitivity of permeance coefficients of penetrants to temperature (expressed through the E_p) increases for those with lower permeability.[65] In this sense, the E_p of permeation would be higher for N_2 than for CO_2. Therefore, the CO_2/N_2 separation selectivity decreases with increasing temperature, as observed in Fig. 5a and b. In addition, it must be taken into account that permeance is the product of solubility and diffusivity and that diffusivity increases with temperature for all gases, which is translated into an increase of permeance for all the membranes. Such diffusion variation is relatively similar for CO_2 and N_2 whose molecular size is very close; however, the solubility of CO_2 in all the actors (PEBA polymer, IL and ZIF-94) decreases with temperature, which undoubtedly produces the decrease of the CO_2/N_2 selectivity with temperature. The permeation E_p values calculated for the optimal membranes are collected in Table 1 and compared with analogous data found in the literature for dense membranes (since, as far as we know, Pebax® TFC/TFN membranes have not been studied as a function of temperature). As observed in this table, the values of the CO_2 and N_2 activation energies of the TFC_PEBA membrane are in accordance with those reported in the literature for several Pebax® codes. Moreover, as expected, the E_p of N_2 (30.1 kJ mol^{-1}) is much higher than that of CO_2 (11.7 kJ mol^{-1}). It is worth mentioning that the CO_2 E_p for the TFC_PEBA(10IL) membrane is *ca.* two times lower (5.3 kJ mol^{-1}) than that for the TFC_PEBA membrane (11.7 kJ mol^{-1}). This behavior was already observed by Rabiee *et al.*,[57] who evaluated the effect of feed temperature on gas permeability and selectivity of PEBA/[Emim][BF_4] gel membranes and estimated the E_p for permeation of CO_2 and N_2 as a function of the IL content. They found that the E_p decreased with the increase of IL content for all penetrants. This observation is consistent with the fact that the permeations of CO_2 and N_2 increase with the addition of IL. Interestingly, the membrane with 15 wt% of ZIF-94 (SALE) provided and intermediate CO_2 E_p (7.0 kJ mol^{-1}) with similar N_2 E_p than the TFC_PEBA(10IL) membrane, in agreement with the less abrupt loss of CO_2/N_2 separation selectivity as a function of temperature for the membrane with the IL and the ZIF (Fig. 5b) related to the lower N_2 E_p − CO_2 E_p difference of 12.7 kJ mol^{-1}. All these results suggest that the temperature increase of permeation is affected by both the addition of IL and incorporation of ZIF nanoparticles. Specially, the decrease in selectivity with temperature is different depending on the membrane, which undoubtedly indicates that the introduction of IL and/or ZIF-94 changes the transport properties of the membranes. It is worth mentioning that measurement error may be the cause of the lower selectivity accounted for TFC PEBA(10IL) than for TFC PEBA at 25 °C, which would be expected to be higher as found at 35 °C. In fact, the error bar in selectivity is around 3–10%, as seen in Fig. 4a, suggesting that Fig. 5b represents with the needed accuracy the change in selectivity as a function of temperature and membrane type.

Table 1 Apparent activation energies for permeation of CO_2 and N_2

	E_p CO_2	E_p N_2	
Membrane	kJ mol^{-1}		Ref
Pebax® 1657	13.3	30.4	66
Pebax® 1657	14.9	28.0	64
Pebax® 1657	14.6	33.6	67
Pebax® 2533	16.7	27.2	68
Pebax® 2533	18.2	31.0	69
Pebax® 3533	14.2	29.6	70
Pebax® 1074	13.4	30.3	44
TFC_PEBA	11.7	30.1	This work
TFC_PEBA(10IL)	5.3	19.6	This work
TFC_PEBA(10IL)_ZIF94(15)	7.0	19.7	This work

3.3.4. Long-term stability studies. PTMSP is a highly permeable glassy polymer that possesses an unrelaxed free fractional volume (FFV) and due to that undergoes physical aging because of the chain rearrangement, resulting in the reduction of the membrane permeance.[71] Therefore, one major concern when using this polymer as gutter layer is its aging. Chen *et al.*[72] demonstrated that a thin coating of PTMSP can lose up to 80% of the CO_2 permeance within 14 days. In this work, the long-term stability of the optimal membranes was tested for 18 days at 35 °C and 3 bar feed pressure. It must be noted that during the long-term stability tests, the membranes

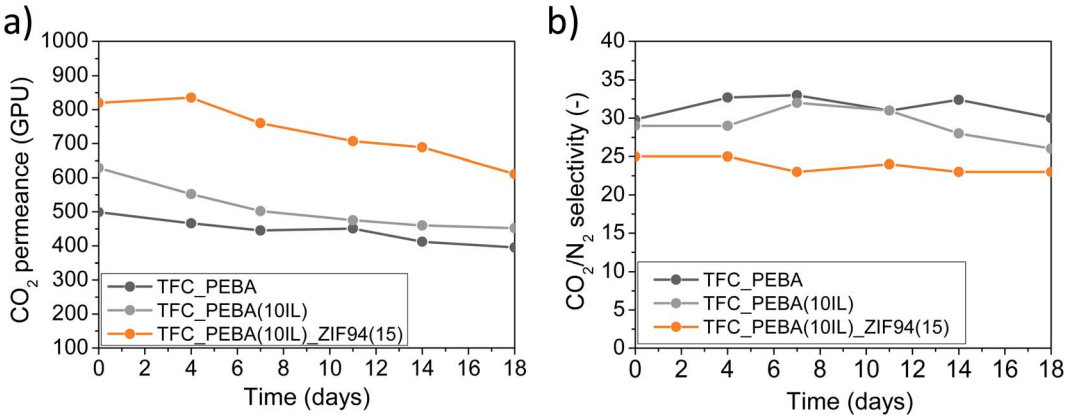

Fig. 6 Long-term stability of the TFC and TFN membranes prepared in this work. Measured at 35 °C and 3 bar feed pressure; CO_2 permeance (a) and CO_2/N_2 selectivity (b).

were periodically exposed to the gas mixture and stored, coupled in the membrane module, at RT between each measurement. In the open literature, other authors attempted to study the long-term stability of Pebax® membranes. Lee *et al.*[73] studied the stability of Pebax® 2333 TFC membranes for 36 days, without changes in the separation performance. Shin *et al.*[74] tested the long-term stability of a dense Pebax® 1657/PEG/GO MMM for 100 days, observing that after such period of time the membranes did not show evidence of aging. Although these papers evaluate the stability of the membranes for longer periods of time, these configurations did not incorporate an ionic liquid, which highly affects the aging of the membrane, as found in this work. Pardo *et al.*[75] evaluated the long-term stability of a Pebax® 1657/IL dense membrane for 25 days with stable behavior; however, their aim was to separate a refrigerant blend instead of a CO_2/N_2 mixture. Having said this, Fig. 6 indicates that the membranes gradually lose their permeance along the 18 days of testing. The maximum loss of permeance was experienced by the TFC_PEBA(10IL) membrane, which decreased its CO_2 permeance by 28%, from 629 GPU to 460 GPU followed by the membrane with ZIF-94 (membrane TFC_PEBA(10IL)_ZIF94(15)), whose CO_2 permeance decreased by 25% (from 820 GPU to 611 GPU). The pristine TFC membrane lost a 20% of its CO_2 permeance (from 497 GPU to 395 GPU). Considering these results, it is noticeable that the IL worsens the stability of the membranes, which can be associated with the increment in the mass transport velocity as well as the exudation followed by the displacement of the IL through the membrane.[76] Nevertheless, such deterioration was mitigated with the incorporation of ZIF-94, which partially avoids the exudation of the IL. Due to their chemical affinity based on their common imidazole species, IL [Bmim][BF_4] should interact more strongly with ZIF-94 than with the polymer. In consequence, the ZIF-94 is trapped in the polymer matrix as an anchor point for the IL enhancing its stability in the TFN membrane. In this sense and to gain insight into the stability of the membranes for longer periods of time, a linear regression was carried out with the data of CO_2 permeance and operation time (as explained in the ESI†), obtaining a good fitting in all configurations, as depicted in Fig. S2,† allowing the estimation of the half-life time of each configuration. As collected in Table S4,† the time at which the CO_2 permeance of the membrane with a 10 wt% of IL was reduced by half is 23 days, whereas that of the membrane that incorporates ZIF-94 is prolonged to 39 days, which is closer to the time achieved with the pristine membrane (44 days). In agreement with this, despite the loss of performance after 18 days of tests, it is worth mentioning that the CO_2 permeance decrease is far from the values previously reported by Chen *et al.*[72] for thin film coatings of PTMSP without selective layer where the reduction in permeance was 80% in 14 days compared to the 20–28% reduction represented here in a similar period of time. The improvement in the long-term stability of the membranes can be also due to the partial penetration of the Pebax® chains into the PTMSP gutter layer, meaning that polymeric chains for both polymers could be intertwined, stabilizing the non-equilibrium PTMSP structure.[77] In any event, after 18 days of separation activity membrane TFC_PEBA(10IL)_ZIF94(15) is 55% and 35% more permeable than the bare polymer and the membrane with only IL maintaining a CO_2/N_2 separation selectivity of 25.

3.3.5. Comparison with other TFC and TFN membranes that contain Pebax® and IL. The CO_2/N_2 separation performance of the membranes prepared in this work has been compared with those of other TFC and TFN membranes found in the literature containing IL.[27,37,78–80] As seen in Table 2, Fam *et al.*[37] obtained a similar CO_2/N_2 separation performance that the one obtained in this work with the TFC_PEBA(10IL) membrane by incorporating GO and [Emim][BF_4] IL into Pebax® 1657. Nevertheless, it is worth mentioning that they fabricated hollow fibers (HF) instead of flat sheet membranes, as reported in this work. Additionally, to obtain similar results, they needed from the addition of graphene oxide (GO) to the solution, since the CO_2 permeance of the Pebax®/IL HF itself only reached up to 300 GPU, as reported previously.[79] Rhyu *et al.*[78] also prepared TFC membranes with [Bmim][BF_4] but using Pebax® 2533 instead of Pebax® Renew® 30R51. With this membrane, they obtained a CO_2 permeance of 101 GPU and a CO_2/N_2 selectivity of 42. Finally, De Dai *et al.*[80] prepared a TFC membrane with a Pebax®/task-specific ionic liquid (TSIL) blend selective layer coated on top of a PSF ultrafiltration support and

Table 2 Comparison with other TFC and TFN membranes containing Pebax® and IL

Membrane	CO_2 permeance (GPU)	CO_2/N_2 selectivity	Ref
Pebax®2533/[Bmim][BF_4]	101	42	78
Pebax®1657/GO-IL	905	45	27
Pebax®1657/[Emim][BF_4]/GO[a]	642	34	37
Pebax®1657/[Emim][BF_4][a]	300	36	79
Pebax®2533/TSIL	250	30	80
TFC_PEBA	497	27	This work
TFC_PEBA(10IL)	629	29	This work
TFC_PEBA(10IL)_ZIF8(15)	751	25	This work
TFC_PEBA(10IL)_ZIF94(15)	819	25	This work

[a] Hollow fibers.

studied its CO_2 separation performance as a function of the relative humidity (RH). At 0% RH (which is the condition used in this research), they reached up to 250 GPU of CO_2 and a CO_2/N_2 selectivity of 30. In any event, the closest situation to our TFN membranes includes Pebax® 1657/graphene oxide-IL TFN membranes,[27,37] whose stability was studied for only up to 28 h.[37]

3.3.6. CO_2/CH_4 separation performance. To further complete this work, the CO_2/CH_4 separation performance of the optimal membranes prepared in terms of CO_2/N_2 (TFC_PEBA, TFC_PEBA(10IL) and TFC_PEBA(10IL)_ZIF94(15)) was studied and the results obtained are depicted in Fig. S3.† As observed in this figure, the membranes followed a similar trend for the separation of CO_2 from CH_4 than from N_2, enhancing the CO_2 permeance with the incorporation of IL and ZIF-94 without affecting the separation selectivity. In fact, the CO_2 permeance increased from 581 GPU to 689 GPU after the addition of 10 wt% of IL, and to 838 GPU after the incorporation of both, 10 wt% of IL and 15 wt% of ZIF-94 (SALE), which means improvements of 19% and 48%, respectively. As mentioned, the CO_2/CH_4 selectivity was maintained at a value of 10, considerably lower than the CO_2/N_2 selectivity in line with the general behavior of PEBA type polymers.[54]

4. Conclusions

Pebax® Renew® 30R51 TFC membranes and ZIF-8 or ZIF-94/IL/Pebax® Renew® TFN membranes were prepared and characterized for CO_2/N_2 separation. ZIF-94 was prepared *via* a solvent assisted ligand exchange (SALE) reaction using ZIF-8 as a precursor material suspended in 1-butanol. The high extension of the ligand exchange was confirmed by TGA, DTG, XRD, FTIR and BET analyses. The addition of [Bmim][BF_4] into the Pebax® Renew® composite membranes enhanced the CO_2 separation performance of the membranes up to 10 wt% of loading, reaching a CO_2 permeance of 629 GPU and a CO_2/N_2 selectivity of 29, which means increases of 27% and 11% compared with the CO_2 permeance and the CO_2/N_2 separation selectivity of the pristine membrane, respectively. The incorporation of ZIF-8 or ZIF-94 particles into the IL/Pebax® matrix also improved the CO_2 permeance of the membranes over the ones which only had IL, which was attributed to the improved compatibility between ZIFs and the polymer matrix due to the presence of the IL. For both ZIFs, the best gas separation results were obtained at 15 wt% of ZIF loading and 10 wt% of IL, reaching CO_2 permeances of 751 GPU and 819 GPU for ZIF-8 and ZIF-94, respectively, together with a CO_2/N_2 selectivity of 25 in both cases. It is worth mentioning that it was for up to 15 wt% of ZIF loading that the membranes with ZIF-94 were more permeable than those with ZIF-8. This behavior was attributed to the CO_2-philic nature of ZIF-94, due to its aldehyde group which in turn increases its hydrophilicity and compatibility with the polymer and the IL. In addition, the apparent activation energies of permeation were also calculated for the optimal membranes, obtaining similar results to those reported in the literature for Pebax® type copolymer with the pristine TFC membrane, but lower values with the membranes with IL and IL/ZIF-94. These results were related to the increment of CO_2 and N_2 permeation, clearly supporting the positive influence of IL and ZIF on the diffusion and solubility properties of the membranes with respect to the pure polymer.

The long-term stability of the membranes was studied for 18 days. Results indicated that the IL affected the stability of the membrane increasing the CO_2 permeance loss from 20% to 28%. However, the incorporation of ZIF-94 partially mitigated such deterioration reaching a CO_2 permeance loss of 25% after 18 days of testing. In spite of the fact that the long-term stability of the membranes was affected by the use of PTMSP as a gutter layer, the CO_2 permeance loss was far from previous results found in the literature. In any event, after the 18 days of continuous performance, the membrane with IL and ZIF-94 was 55% and 35% more CO_2 permeable than the bare polymer and the membrane with only IL, respectively, maintaining a CO_2/N_2 separation selectivity of 25.

Conflicts of interest

There are no conflicts to declare.

Acknowledgements

Grants PID2019-104009RB-I00 funded by MCIN/AEI/10.13039/501100011033 is gratefully acknowledged (Agencia Estatal de Investigación (AEI) and MCIN (Ministerio de Ciencia e

Innovación), Spain). Grant T43-20R financed by the Aragón Government is gratefully acknowledged. L. Martínez-Izquierdo also thanks the Aragón Government (DGA) for her PhD grant. The authors would like to acknowledge the use of Servicio General de Apoyo a la Investigación (SAI) and the use of instrumentation as well as the technical advice provided by the National Facility ELECMI ICTS, node "Laboratorio de Microscopias Avanzadas" at the University of Zaragoza.

References

1 Y. Zhang, J. Sunarso, S. Liu and R. Wang, *Int. J. Greenhouse Gas Control*, 2013, **12**, 84–107.
2 N. Saini and K. Awasthi, *Sep. Purif. Technol.*, 2022, **282**, 120029.
3 N. H. Solangi, A. Anjum, F. A. Tanjung, S. A. Mazari and N. M. Mubarak, *J. Environ. Chem. Eng.*, 2021, **9**, 105860.
4 B. Zhu, S. He, Y. Wu, S. Li and L. Shao, *Engineering*, DOI: DOI: 10.1016/J.ENG.2022.03.016.
5 S. He, B. Zhu, X. Jiang, G. Han, S. Li, C. H. Lau, Y. Wu, Y. Zhang and L. Shao, *Proc. Natl. Acad. Sci. U. S. A.*, 2022, **119**, e2114964119.
6 S. Ding, X. Li, S. Ding, W. Zhang, R. Guo and J. Zhang, *Sep. Purif. Technol.*, 2020, **239**, 116539.
7 A. Brunetti, F. Scura, G. Barbieri and E. Drioli, *J. Membr. Sci.*, 2010, **359**, 115–125.
8 W. Yave, A. Car, J. Wind and K.-V. Peinemann, *Nanotechnology*, 2010, **21**, 7.
9 L. M. Robeson, *J. Membr. Sci.*, 2008, **320**, 390–400.
10 A. Guo, Y. Ban, K. Yang, Y. Zhou, N. Cao, M. Zhao and W. Yang, *J. Membr. Sci.*, 2020, **601**, 117880.
11 J. Dechnik, J. Gascon, C. J. Doonan, C. Janiak and C. J. Sumby, *Angew. Chem., Int. Ed.*, 2017, **56**, 9292–9310.
12 F. Amirkhani, M. Mosadegh, M. Asgharia and M. J. Parnian, *Polym. Test.*, 2020, **82**, 106285.
13 D. Peng, S. Wang, Z. Tian, X. Wu, Y. Wu, H. Wu, Q. Xin, J. Chen, X. Cao and Z. Jiang, *J. Membr. Sci.*, 2017, **522**, 351–362.
14 T.-C. Huang, Y.-C. Liu, G.-S. Lin, C.-H. Lin, W.-R. Liu and K.-L. Tung, *J. Membr. Sci.*, 2020, **602**, 117946.
15 S. Zhang, Y. Zheng, Y. Wu and B. Zhang, *J. Appl. Polym. Sci.*, 2021, **138**, 51336.
16 Y. Zheng, Y. Wu, B. Zhang and Z. Wang, *J. Appl. Polym. Sci.*, 2020, 48398.
17 J. Sánchez-Laínez, I. Gracia-Guillé, B. Zornoza, C. Téllez and J. Coronas, *New J. Chem.*, 2019, **43**, 312–319.
18 P.-H. Tang, P. B. So, W.-H. Li, Z.-Y. Hui, C.-C. Hu and C.-H. Lin, *Membranes*, 2021, **11**, 404.
19 Y. Shi, S. Wu, Z. Wang, X. Bi, M. Huang, Y. Zhang and J. Jin, *Sep. Purif. Technol.*, 2021, **277**, 119449.
20 M. Benzaqui, M. Wahiduzzaman, H. Zhao, M. R. Hasan, T. Steenhaut, A. Saad, J. Marrot, E. Normand, J.-M. Grenèche, N. Heymans, G. De Weireld, A. Tissot, W. Shepard, Y. Filinchuk, S. Hermans, F. Carn, M. Manlankowska, C. Téllez, J. Coronas, G. Maurin, N. Steunou and C. Serre, *J. Mater. Chem. A*, 2022, **10**, 8535–8545.
21 M. Benzaqui, R. Semino, N. Menguy, F. Carn, T. Kundu, J.-M. Guigner, N. B. Mckeown, K. J. Msayib, M. Carta, R. Malpass-Evans, ⊥ Clément, C. Le Guillouzer, G. Clet, N. A. Ramsahye, C. Serre, G. Maurin and N. Steunou, *ACS Appl. Mater. Interfaces*, 2016, **8**, 27311–27321.
22 M. van Essen, R. Thür, L. van den Akker, M. Houben, I. F. J. Vankelecom, K. Nijmeijer and Z. Borneman, *J. Membr. Sci.*, 2021, **637**, 119642.
23 Z. Guo, W. Zheng, X. Yan, Y. Dai, X. Ruan, X. Yang, X. Li, N. Zhang and G. He, *J. Membr. Sci.*, 2020, **605**, 118101.
24 F. Galiano, R. Mancuso, L. Guazzelli, M. Mauri, C. Chiappe, R. Simonutti, A. Brunetti, C. S. Pomelli, G. Barbieri, B. Gabriele and A. Figoli, *J. Membr. Sci.*, 2021, **635**, 119479.
25 C. Hermida-Merino, F. Pardo, G. Zarca, J. M. M. Araújo, A. Urtiaga, M. M. Piñeiro and A. B. Pereiro, *Nanomater*, 2021, **11**, 607.
26 J. Lu, X. Zhang, L. Xu, G. Zhang, J. Zheng, Z. Tong, C. Shen and Q. Meng, *Membr*, 2021, **11**, 35.
27 G. Huang, A. P. Isfahani, A. Muchtar, K. Sakurai, B. B. Shrestha, D. Qin, D. Yamaguchi, E. Sivaniah and B. Ghalei, *J. Membr. Sci.*, 2018, **565**, 370–379.
28 A. Jomekian, B. Bazooyar, R. M. Behbahani, T. Mohammadi and A. Kargari, *J. Membr. Sci.*, 2017, **524**, 652–662.
29 C. Casado-Coterillo, A. Fernández-Barquín, B. Zornoza, C. Téllez, J. Coronas and Á. Irabien, *RSC Adv.*, 2015, **5**, 102350–102361.
30 M. T. Vu, R. Lin, H. Diao, Z. Zhu, S. K. Bhatia and S. Smart, *J. Membr. Sci.*, 2019, **587**, 117157.
31 S. Aguado, J. Canivet and D. Farrusseng, *Chem. Commun.*, 2010, **46**, 7999–8001.
32 W. Morris, N. He, K. G. Ray, P. Klonowski, H. Furukawa, I. N. Daniels, Y. A. Houndonougbo, M. Asta, O. M. Yaghi and B. B. Laird, *J. Phys. Chem. C*, 2012, **116**, 24084–24090.
33 L. A. Neves, N. Nemestóthy, V. D. Alves, P. Cserjési, K. Bélafi-Bakó and I. M. Coelhoso, *Desalination*, 2009, **240**, 311–315.
34 Y. Jiang, Y. Wu, W. Wang, L. Li, Z. Zhou and Z. Zhang, *Chin. J. Chem. Eng.*, 2009, **17**, 594–601.
35 X. Yan, S. Anguille, M. Bendahan and P. Moulin, *Sep. Purif. Technol.*, 2019, **222**, 230–253.
36 K. Friess, P. Izák, M. Kárászová, M. Pasichnyk, M. Lanč, D. Nikolaeva, P. Luis and J. C. Jansen, *Membr*, 2021, **11**, 97.
37 W. Fam, J. Mansouri, H. Li, J. Hou and V. Chen, *ACS Appl. Mater. Interfaces*, 2018, **10**, 7389–7400.
38 T. Johnson, M. M. Łozińska, A. F. Orsi, P. A. Wright, S. Hindocha and S. Poulston, *Green Chem.*, 2019, **21**, 5665–5670.
39 H. Li, L. Tuo, K. Yang, H. K. Jeong, Y. Dai, G. He and W. Zhao, *J. Membr. Sci.*, 2016, **511**, 130–142.
40 Z. Yang, Y. Ying, Y. Pu, D. Wang, H. Yang and D. Zhao, *Ind. Eng. Chem. Res.*, 2022, **61**, 7626–7633.
41 J. Sánchez-Laínez, B. Zornoza, S. Friebe, J. Caro, S. Cao, A. Sabetghadam, B. Seoane, J. Gascon, F. Kapteijn, C. Le Guillouzer, G. Clet, M. Daturi, C. Téllez and J. Coronas, *J. Membr. Sci.*, 2016, **515**, 45–53.
42 D. Madhav, M. Malankowska and J. Coronas, *New J. Chem.*, 2020, **44**, 20449–20457.

43 A. M. Marti, M. Van and K. J. Balkus, *J. Porous Mater.*, 2014, **21**, 889–902.
44 L. Martínez-Izquierdo, M. Malankowska, C. Téllez and J. Coronas, *J. Environ. Chem. Eng.*, 2021, **9**, 105624.
45 C. W. Tsai, J. W. Niemantsverdriet and E. H. G. Langner, *Microporous Mesoporous Mater.*, 2018, **262**, 98–105.
46 M. Etxeberria-Benavides, O. David, T. Johnson, M. M. Łozińska, A. Orsi, P. A. Wright, S. Mastel, R. Hillenbrand, F. Kapteijn and J. Gascon, *J. Membr. Sci.*, 2018, **550**, 198–207.
47 F. Cacho-Bailo, M. Etxeberría-Benavides, O. Karvan, C. Téllez and J. Coronas, *CrystEngComm*, 2017, **19**, 1545–1554.
48 V. Berned-Samatán, C. Rubio, A. Galán-González, E. Muñoz, A. M. Benito, W. K. Maser, J. Coronas and C. Téllez, *J. Membr. Sci.*, 2022, **652**, 120490.
49 M. R. Hasan, L. Paseta, M. Malankowska, C. Téllez and J. Coronas, *Adv. Sustainable Syst.*, 2021, 2100317.
50 F. Akbari Beni and M. Niknam Shahrak, *Polyhedron*, 2020, **178**, 114338.
51 M. Kattula, K. Ponnuru, L. Zhu, W. Jia, H. Lin and E. P. Furlani, *Sci. Rep.*, 2015, **5**, 1–9.
52 T. Li, Y. Pan, K. V. Peinemann and Z. Lai, *J. Membr. Sci.*, 2013, **425–426**, 235–242.
53 J. Sánchez-Laínez, M. Ballester-Catalán, E. Javierre-Ortín, C. Téllez and J. Coronas, *Dalton Trans.*, 2020, **49**, 2905–2913.
54 A. Selomon, L. Martínez-Izquierdo, M. Malankowska, C. Téllez and J. Coronas, *Energy Fuels*, 2021, **35**, 17085–17102.
55 J. P. Sheth, J. Xu and G. L. Wilkes, *Polymer*, 2003, **44**, 743–756.
56 T. Yoshida, T. Nakane, M. Uchida and Y. Kaneko, *Int. J. Solids Struct.*, 2022, **239–240**, 111419.
57 H. Rabiee, A. Ghadimi and T. Mohammadi, *J. Membr. Sci.*, 2015, **476**, 286–302.
58 Q. Luo and E. Pentzer, *ACS Appl. Mater. Interfaces*, 2020, **12**, 5169–5176.
59 K. Friess, J. C. Jansen, F. Bazzarelli, P. Izák, V. Jarmarová, M. Kačírková, J. Schauer, G. Clarizia and P. Bernardo, *J. Membr. Sci.*, 2012, **415–416**, 801–809.
60 A. Husna, I. Hossain, I. Jeong and T. H. Kim, *Polymers*, 2022, **14**, 655.
61 K. M. Gupta, Z. Qiao, K. Zhang and J. Jiang, *ACS Appl. Mater. Interfaces*, 2016, **8**, 13392–13399.
62 S. Gadipelli, W. Travis, W. Zhou and Z. Guo, *Energy Environ. Sci.*, 2014, **7**, 2232–2238.
63 D. Liu, J. Gu, Q. Liu, Y. Tan, Z. Li, W. Zhang, Y. Su, W. Li, A. Cui, C. Gu and D. Zhang, *Adv. Mater.*, 2014, **26**, 1229–1234.
64 L. Martínez-Izquierdo, M. Malankowska, J. Sánchez-Laínez, C. Téllez and J. Coronas, *R. Soc. Open Sci.*, 2019, **6**, 190866.
65 A. Ghadimi, M. Amirilargani, T. Mohammadi, N. Kasiri and B. Sadatnia, *J. Membr. Sci.*, 2014, **458**, 14–26.
66 A. Tena, S. Shishatskiy and V. Filiz, *RSC Adv.*, 2015, **5**, 22310.
67 J. H. Kim, Y. Ha and Y. M. Lee, *J. Membr. Sci.*, 2001, **190**, 179–193.
68 M. M. Rahman, V. Filiz, S. Shishatskiy, C. Abetz, S. Neumann, S. Bolmer, M. M. Khan and V. Abetz, *J. Membr. Sci.*, 2013, **437**, 286–297.
69 E. Tocci, A. Gugliuzza, L. De Lorenzo, M. Macchione, G. De Luca and E. Drioli, *J. Membr. Sci.*, 2008, **323**, 316–327.
70 S. Feng, J. Ren, D. Zhao, H. Li, K. Hua, X. Li and M. Deng, *J. Energy Chem.*, 2019, **28**, 39–45.
71 D. Bakhtin, S. Bazhenov, V. Polevaya, E. Grushevenko, S. Makaev, G. Karpacheva, V. Volkov and A. Volkov, *Membr*, 2020, **10**, 419.
72 H. Z. Chen, Z. Thong, P. Li and T. S. Chung, *Int. J. Hydrogen Energy*, 2014, **39**, 5043–5053.
73 S. Lee, S. C. Park, T. Y. Kim, S. W. Kang and Y. S. Kang, *J. Membr. Sci.*, 2018, **548**, 358–362.
74 J. E. Shin, S. K. Lee, Y. H. Cho and H. B. Park, *J. Membr. Sci.*, 2019, **572**, 300–308.
75 F. Pardo, G. Zarca and A. Urtiaga, *J. Membr. Sci.*, 2021, **618**, 118744.
76 A. R. Nabais, L. A. Neves and L. C. Tomé, *ACS Appl. Polym. Mater.*, 2021, **4**, 3098–3119.
77 P. D. Sutrisna, J. Hou, H. Li, Y. Zhang and V. Chen, *J. Membr. Sci.*, 2017, **524**, 266–279.
78 S. Y. Rhyu and S. W. Kang, *J. Ind. Eng. Chem.*, 2021, **103**, 216–221.
79 W. Fam, J. Mansouri, H. Li and V. Chen, *J. Membr. Sci.*, 2017, **537**, 54–68.
80 Z. De Dai, L. Bai, K. N. Hval, X. P. Zhang, S. J. Zhang and L. Y. Deng, *Sci. China: Chem.*, 2016, **59**, 538–546.